SOME APPLICATIONS OF EFFECTIVE REFRACTION INDEX DESCRIPTION TO PLASMONIC WAVEGUIDES

D.A. Smirnova

Nizhny Novgorod State University

Surface plasmons are widely discussed in last decade as an electromagnetic excitation which could provide light nanofocusing [1]. In our report we draw our attention to some features of plasmon localization in metal-dielectric-metal (MDM) inhomogeneous slot waveguides of two different types: step-wise and smooth. First of all, we discuss the validity framework of effective refraction index approximation and then analyze dispersion equations for most strongly localized fundamental plasmonic modes in both cases.

From integral Maxwell's equations, bearing in mind quasi-transverse electromagnetic field structure of plasmon mode inside very thin slot $\Lambda_p \equiv c/\omega_p > d$ of MDM waveguide (ω_p is the electron plasma frequency in metal, d is the half of thickness of the slot, c is the speed of light) and for low enough operating frequencies $\omega << \omega_p$ we come to the single following equation for the slot voltage $U = 2d(x,y)E_x$, where x, y are the lateral Cartesian coordinates in the plane of the waveguide slot:

$$\frac{\partial^2 U}{\partial x^2} + \frac{\partial^2 U}{\partial y^2} + k_0^2 \varepsilon_{eff}(x,y)U = 0, \quad \varepsilon_{eff} = \frac{\Lambda_p}{d}\varepsilon_0, \tag{1}$$

where ε_0 is the permittivity of a dielectric in the slot, $k_0 = \omega/c$. It should be noted that we might derive the boundary conditions at the abrupt change of the slot thickness: U, $\partial U/\partial n$ are continuous, where $\mathbf{n}$ is the normal direction to the surface of the slot thickness jump in (y,z) plane. Similar approximate effective impedance boundary conditions have also been used in [2]. But strictly speaking, the above boundary conditions provide electromagnetic field connection only at some distance (just of the same order as the step value of the slot thickness) from the thickness jump that ensures the evanescence of the local field.

Equation (1) shows that any narrowing waveguide, leading in its turn to the local growth of effective dielectric permittivity ε_{eff}, may trap the plasmons and form a laterally localized plasmonic eigenmode. As the first example of 2D

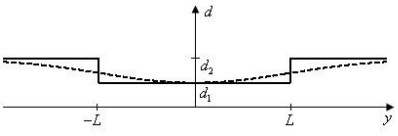

Fig. 1

plasmon localization we consider the straight MDM slot waveguide with rectangular narrowing of the width $2L$ (Fig. 1).

Using the effective boundary conditions one can easily obtain dispersion equations for plasmon eigenmodes. Lateral fundamental eigenmode width has a minimum versus L:

$$\Lambda_{\perp}^{(\min)} \sim 4.9k_0^{-1}\sqrt{\frac{d_1 d_2}{(\varepsilon_1 d_2 - \varepsilon_2 d_1)\Lambda_p}},$$

the solid curve demonstrating this fact in Fig.2, where $\frac{d_2}{d_1} = 2$, L_n and Λ_n are normalized in compliance with the following formulas: $L_n = k_0 L\sqrt{\frac{\Lambda_p \varepsilon_0}{d_1}}, \Lambda_n = k_0\Lambda\sqrt{\frac{\Lambda_p \varepsilon_0}{d_1}}$.

The plasmon eigenmode in smoothly inhomogeneous MDM slot waveguide (dashed line in Fig.1) is considered as the second example assuming:

$$\frac{\Lambda_p}{d} = A + \frac{B}{\cosh^2(y/L)};\ A = \frac{\Lambda_p}{d_2},\ B = \Lambda_p\left(\frac{1}{d_1} - \frac{1}{d_2}\right);\ d_2 > d_1.$$

The transverse structure of the fundamental mode can be expressed via a hyperbolic primitive function. The plot of plasmon eigenmode transverse width as a function of characteristic inhomogineity of waveguide is shown in Fig.2 by dashed line. Simple estimations of $\Lambda_{\perp}^{(\min)}$ at $\varepsilon_0 = 8$, and $\Lambda_p/d_1 = 3$ give $\Lambda_{\perp} \sim$ 100 nm at $\lambda_0 = 2\pi/k_0 = 1550$ nm and $L \sim 50$ nm.

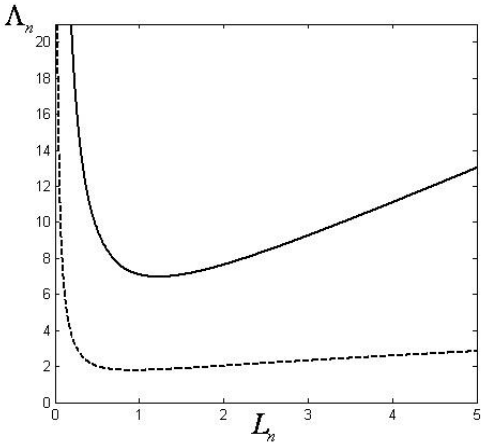

Fig. 2

Summarizing up, we have shown that local narrowing the plasmonic MDM slot waveguide can trap plasmons into 2D localized eigenmodes and squeeze them in the transverse direction. The two types of narrowing (step-wise and smooth) were considered. The plasmon localization scale depends on both the transverse profile of the slot and its characteristic width and it can achieve the value of several tens of nanometers in the near-infrared domain.

[1] Maier S.A. Plasmonics: Fundamentals and Applications. – Berlin: Springer-Verlag, 2007.
[2] Veronis G. and Fan S. //Appl. Phys. Lett. 2005. V.87. P.131102.

THE USE OF A PORTABLE VIBRATOR AND DIGITAL SEISMIC STATION FOR SURFACE LAYERS PROBING

A.I.Konkov[1,2], A.V. Lebedev[2], S.A. Manakov[2]

[1]*Nizhny Novgorod State University*
[2]*Institute of Applied Physics of RAS*

The problem of surface layers profiling is one of the most significant in seismic survey. In this paper we intend to demonstrate how the use of portable vertical vibrator and digital seismic station can help us to solve it.

For seismic waves launching the terrestrial broadband radiator of electrodynamic type was used. Emitted pulse signal was generated by program and was applied to the radiator through the matching circuit. Reception of signals was made with digital multichannel station Lakkolit X-M2. Receiving geophones were placed in a line, pairwise vertical and horizontal ones with 1 m distance between the pairs positions creating a receiving track for each location of the vibrator. Each track length of 23 m contained 24 pairs of geophones. To increase the signal to noise ratio a coherent accumulation of impulse responses together with digital filtering in the band of sounding signals (70–350 Hz) were performed.

Received signal contains different wave packets. Deciphering of whole response was focused on Rayleigh wave analysis. To specify the wave's kinematic characteristics the cross-correlation function of the received signal and the impulse response of the vibrator were calculated. The received signal gating made with use of sliding window method allowed us to extract the response of the Rayleigh wave and determine the vertical and horizontal displacements.

Seismograms corresponding to the whole response (Fig.) were based on experimental data we received from vertical and horizontal geophones (shadow patterns which depict only upper half-cycles). The whole response includes arrivals of different wave types: reflected, refracted, etc. Vector method provided the possibility of their definition.

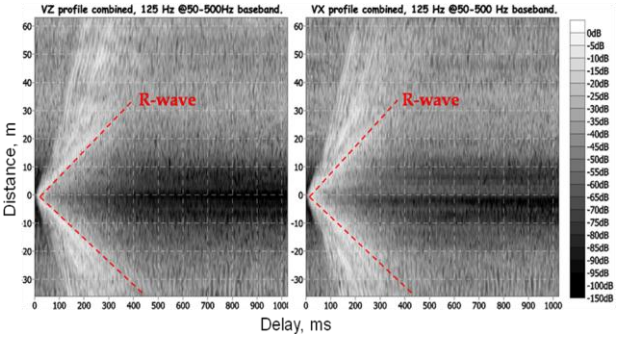

Fig.

The problem of Rayleigh wave verification (the corresponding locus in Fig. indicated by a black dotted line) was quite simple due to several reasons. The first, the «Rayleigh wave line» has the weakest slope corresponding to the lowest velocity of propagation (among all the wave types observed). The second, it stands out because of its brightness (which is consistent with a well-known fact: a Rayleigh wave accumulates the largest part of energy). And finally the third, the kinematic characteristics received from with horizontal and vertical geophones were also used for Poisson's ratio estimation: the obtained value 0,26 is in good agreement with [1] that is an additional proof of correctness of the supposition indicated above.

Theoretical calculations of longitudinal and transverse projections of the displacement were performed with use of [2]. In our case the vibrator was considered as a power source with the pressure uniformly distributed on a circular platform. Rayleigh wave velocity was also estimated by an impulse response of the vibrator and found to be approximately 160 m/c thereby it is in good agreement with [1].

[1] Аки К., Ричардс П. Количественная сейсмология: теория и методы – М.: Мир, 1983, 520 с.
[2] Lebedev A.V., Beresnev I.A. //Geophysics. 2004. V.69, No.4. P.968.

MODELING THERMAL FIELDS IN POWERFUL TRANSISTORS

E.A. Tarasova, S.V. Obolensky

Nizhny Novgorod State University

Powerful transistors are heated a lot. It’s necessary to develop mathematical models for their design. These models would consider all thermal effects and electron transport, depending upon the temperature.

Transistors working at frequencies 300 GHz are heated very much, that’s why it is important to know the maximum temperature. When it is higher than some definite value, then the device can be burned. Transistor current also depends upon the temperature, this task is self-consistent and difficult for modeling.

Modern transistors have a form of a section for decreasing parasitic induction and resistance. The sections are heating each other. The temperature in the middle of the sections is higher than in their face part, so we need calculating thermal configuration in all the three dimensions. There were no calculations of this type earlier.

In the works [1,2] some analytical and numerical calculations were suggested. The analytical formula was given only in the 2-dimensional approach, without taking into account the distance between the sections; and numerical calculations for infinite number of sections were done. Both models didn’t show an edge effects. The error in calculations by using these methods is more than 50 per cent.

The experimental data is obtained with the help of an infrared pyrometer. For the sections with an external size of about 10 mkm this information could be wrong. That’s why we need some computer-based models.

Numerical calculations take a lot of time and there are many parameters to be watched, such as the material conductance, the depth of a GaAs crystal, geometrical parameters of transistors and others. So, we need to develop an analytic solution for the plenary optimization.

For developing this formula, numerical calculations were conducted by means of two models. The maximum temperature from each section was calculated by the first model, and the temperature from one section was calculated by the second one. The investigating model is presented in Fig. 1 schematically. The mathematical model is based on Laplas formula. The basic parameters were: L_z = 50, 100, 150, and 200 mkm, d = 6,25, 12,5, 25, 37,5 mkm, b=33, 50, 75, 83, 100, 116, 125, 133, 150, 175, 200, 250, 300, 350, 500, 700, 1000 mkm. 320 calculations with the first model and 50 calculations with the second one were made. Such a good selection of calculations helped us to develop the analytical formula:

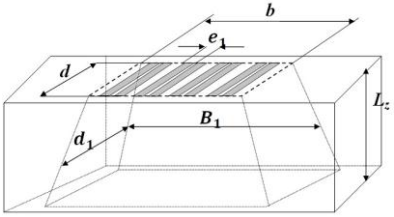

Fig. 1. The experimental model.

$$T = \frac{P \cdot Lz}{B_1 \cdot d_1 \cdot \lambda} \cdot \left(\frac{B_1}{d_1}\right)^k \cdot \left(\frac{B_1 \cdot d_1}{Lz^2}\right)^n \cdot m + T_{base},\ B_1 = b \cdot N + e_1 \cdot (N-1) + Lz,\ d_1 = d + Lz$$

The error from calculations with the use of this formula is 0,1–10 per cent.

The diagrams in Fig. 2 and Fig. 3 show thermal dependences on the thickness of the GaAs crystal, the transistor length, and the transistor area.

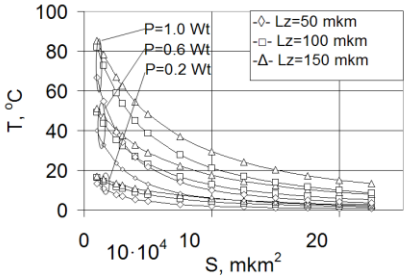

Fig. 2. The relation between the maximum temperature of the transistor and it's geometrical parameters.

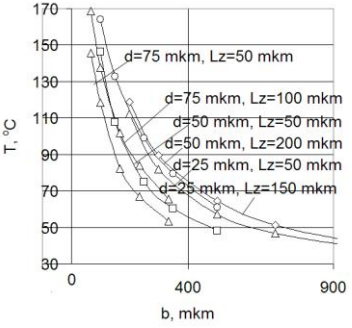

Fig. 3. The relation between the maximum temperature of the transistor and it's length.

Thus, as a result, we have designed the analytical formula which describes all thermal relations.

This formula can be applied for all devices of a section type, such as diodes or bipolar transistors. This methodology is supposed to be applied for High Electron Mobility Transistor solutions.

[1] Shur M. GaAs devices and circuits.– N.Y.: Plenum Press, 1987.
[2] DiLorenzo J.V., Khandelwal D.D. GaAs FET principles and technology. – Dedham, Massachusetts: Artech house, 1982, 773 p.
[3] Moran D.A.J., Kalna K.,. Boyd E, McLelland F., Zhuang L.L., Stanley C.R., Asenov A., Thayne L. // Proc. of the 33rd European Solid-State Device Research. 2003, Estoril, Portugal.

PLASMA CHANNEL WAVE DIAGNOSTICS

A.O. Ryabov, G.A. Markov

Nizhny Novgorod State University

The high-frequency discharge generation together with diagnostic broadband signals shaping and detection of signals traveling away along the plasma channel are the main purposes of the experiment described in this paper.

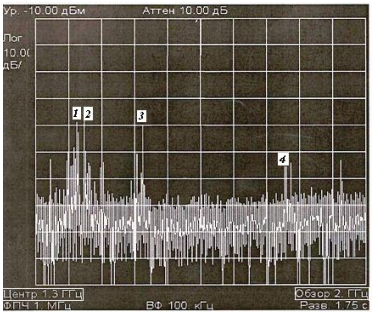

Fig. 1

The glass balloon with the length of 150 cm was filled up with air. The discharge was formed as a result of plasma waves launched with the use of a quadrupole source, which consists of three rings anchored in the central part of the glass balloon. High-frequency voltage was applied to stimulating rings from the generator GST-2 via a coaxial cable. For the diagnostic signal stimulation Rohde-Schwarz generator, a power amplifier and a quadrupole antenna were used.

The spectrogram depicted in Fig. 1 was received for the case, when a plasma pole was absent. It is quite easy to single out the noise terms caused by operating frequencies (indicated by numbers 1–4) of TV and mobile stations.

When we switch on a high-frequency discharge (Fig. 2) we can see a harmonic component corresponding to the main frequency (200 mHz) of pumping field and a harmonic component corresponding to the frequency of a small diagnosic signal (363 mHz), which is marked with the white circle. This signal is too small, so it has no parametric interaction with the pumping one. We could use these spectrograms for plasma diagnostics, if the error probability (generally based on the

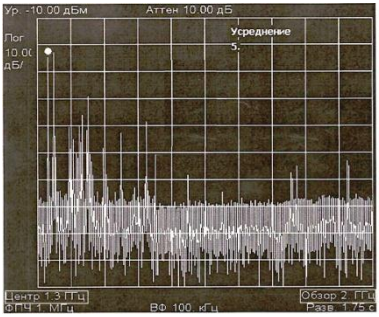

Fig. 2

fact that the pumping field harmonic components can propagate over a free space without plasma) would be smaller.

For correct diagnostics it is preferable to use the waves propagating along the plasma pole [1] so that it is necessary to cut off the harmonic components propagating over free space. This way becomes possible if we compare spectrograms of signals received from the antenna when the diagnostic signal is switched either off or on. In the latter case the received signal consists of harmonic components of the diagnostic signal and the ones formed as a result of cooperation between them and pumping wave harmonics.

When comparing Fig. 2 and Fig. 3, later on we can see that the signals spectra become broader after the operations of connection and amplification. The comparison of signals spectrograms received from the antenna, when the power diagnostic signal is either switched off or on, gives us the way to calculate the blocking frequency in the plasma pole (0,8 gHz; marked as "max" in Fig. 3).

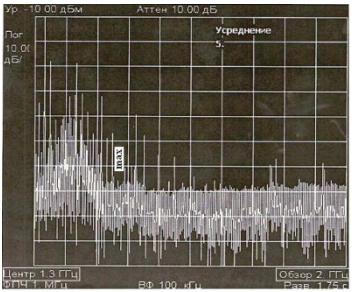

Fig. 3

This method gives us the possibility to estimate the concentration of the magnetoactive plasma disturbed by an external magnetic field.

[1] Ginzburg V.L. Propagation of electromagnetic waves in plasma. – N.Y.: Pergamon Press, 1970.

THRESHOLD OF SELF-INDUCED TRANSPARENCY IN RELATIVISTIC INTERACTION OF AN ELECTROMAGNETIC WAVE WITH OVERDENSE PLASMA LAYER

M.A. Panfilova

Nizhny Novgorod State University

Modern laser technology provides pulses with the intensity of the order of 10^{22} W/cm^{-2}. Thus relativistic and striction nonlinear effects take place in the interaction between laser radiation and plasma. These effects become very important in technical applications, which range from plasma-based particle and photon accelerators to inertial confinement fusion. One of these effects is relativistic self-induced transparency. It implies that if the incident field exceeds the threshold value, the overdense plasma becomes transparent for the radiation due to the relativistic increase of the inertial electron mass and consequent lowering of the natural plasma frequency. The efficiency of the plasma-based charged particles acceleration is higher near this threshold, that is why its determination is of great importance.

A traveling wave approach developed in [1] is commonly used to obtain theoretically the transparency threshold for the infinite homogeneous plasma. But in real situations laser radiation interaction with a plasma boundary is observed. The traveling wave approach is convenient for plasma with a smooth boundary. But in case of plasma with a sharp boundary the nonlinear ponderomotive force generated in the laser-plasma interaction pushes electrons into plasma thus creating strong peaking of the plasma electron density. This results in a suppression of the laser penetration and significant enhancement of the threshold of the penetration. In [2] the analytical threshold of penetration in case of a sharp boundary was essentially modified and a stationary model was developed to derive it for the circularly polarized wave.

The main purpose of the present work is to determine the self-induced transparency threshold in case of the circularly and linearly polarized wave and sharp boundary; and also to compare the numerical and analytical results. The penetration of a superintense laser pulse into the layer of the overdense plasma was simulated using one-dimensional PIC-code. The part of energy passed through the layer depends on the plasma density and the field amplitude. To investigate the transparency threshold, the diagram for energy part passed was obtained, where the region of transparency was determined. The method implies integrating the energy part passed over time in the fixed point behind the plasma layer. The threshold experimentally obtained for circular polarization is in good agreement with the stationary model. But the threshold for linear polarization is significantly lower and is described rather with the plane wave approach. The problem of the difference in question is not easy and will be investigated somewhere else in future.

[1] Akhiezer A.I., Polovin R.V.// Sov. Phys. JETP. 1956. V. 3. P. 696.
[2] Cattani F., Kim A., Anderson D., Lisak M.// Phys. Rev. E. 2000. V.62, No.1. P.1234.

THE USE OF CAPON METHOD FOR AMBIENT NOISE LEVEL ESTIMATION IN THE PRESENCE OF SPATIALLY UNCORRELATED AND LOCALIZED INTERFERENCES

A.S. Ivanenkov, A.A. Rodionov, V.I. Turchin

Institute of Applied Physics of RAS

The level of sea noise is one of the most important parameters that affect the operational range of various hydroacoustic systems (such as sonars). The characteristics of the sea noise tend to change, depending on time and place. They can be different in various water areas, they vary in dependence on season, weather conditions, etc. Thereby, the problem of onsite measurements of ambient noise characteristics is highly actual. In the present paper, the problem of ambient noise level determination with the use of a linear equidistant antenna array will be considered. In the absence of localized noise sources, the problem of noise level estimation is trivial. At the same time, an antenna array can be located near a ship that carries a hydroacoustic system, or can be placed directly on a ship that is a

source of intensive acoustic interference. In addition, a significant contribution to the total power of the measured signal can be made by self-noise of receiving elements and by the hydrodynamic interference caused by ship movement. These circumstances require the development of special methods for sea noise estimation. In the present work, a method for estimating the sea noise level based on the Capon spectral estimate [1] that allows suppressing localized interferences is proposed.

The following model of the received signal is considered. The *jth* time sample at the output of an antenna array after narrowband filtering at frequency f_0 can be represented by the $N\times 1$ vector including three components: $\mathbf{x}_j = \boldsymbol{\tau}_j + \boldsymbol{\xi}_j + \mathbf{s}_j$, $j = 1,..., J$, where N is the number of hydrophones, $\boldsymbol{\tau}_j$ is sea noise, $\boldsymbol{\xi}_j$ is independent noise, $\mathbf{s}_j$ is a localized interference. All the components are supposed to be zero-mean gaussian processes. Hereafter, the component $\boldsymbol{\tau}_j$ will be assumed to be completely isotropic, and its correlation matrix can be presented as follows [2]:

$$\left\langle \boldsymbol{\tau}_j \boldsymbol{\tau}_j^H \right\rangle = \sigma_i^2 \mathbf{T}, \text{ where } \mathbf{T} = \left\| \frac{\sin(kd(n-m))}{kd(n-m)} \right\|_{n,m=\overline{1,N}},$$

where $(\cdot)^H$ denotes the Hermitian transpose, σ_i^2 is the power of isotropic noise, d is the distance between hydrophones, k is the wave number, c is the sound speed in water. The correlation matrix of independent noise is $\left\langle \boldsymbol{\xi}_j \boldsymbol{\xi}_j^H \right\rangle = \sigma_0^2 \mathbf{I}$, where σ_0^2 is the power of independent noise. The correlation matrix of a localized interference is assumed to be unknown.

In the case when the antenna array has a filled aperture and a localized interference is absent, it is easy to obtain the estimates of the σ_0^2 and σ_i^2 from the spatial spectrum levels of real and imaginary angle ranges. In the presence of a powerful localized interference source, using the conventional spatial spectrum leads to a great error in the estimates of σ_0^2 and σ_i^2. In the present work, we use the Capon spectral estimate $f(s_\theta) = (\mathbf{a}(s_\theta)^H \mathbf{R}_x^{-1} \mathbf{a}(s_\theta))^{-1}$ instead, where s_θ is the sine of bearing, $a(s_\theta) = \left\| \exp(ikx_n s_\theta) \right\|_{n=\overline{1,N}}$ is the steering vector, $\mathbf{R}_x^{-1}$ is the estimate of the inverse correlation matrix of the signal. For estimation of powers σ_0^2 and σ_i^2, the direct approximation of the Capon spectrum of the received signal by the model Capon spectrum is used. The model spectrum corresponds to the correlation matrix $\mathbf{R}_m = \sigma_i^2 \mathbf{T} + \sigma_0^2 \mathbf{I}$ which does not include a localized interference component. It has been shown numerically that the error of estimate of the isotropic noise level in the case of using the Capon method is acceptable and tends to a constant when increasing the localized interference power.

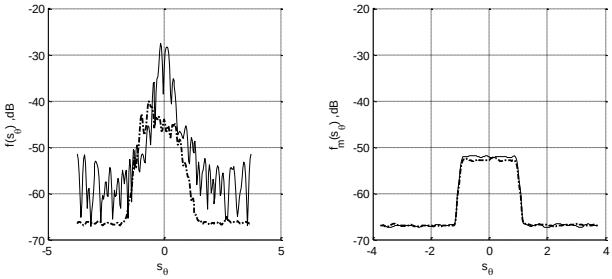

Fig.

In the figure below, the experimental results are presented. They were obtained from the measurements performed in Lake Ladoga in 2009. An antenna array consisting of 64 elements was at the depth of ten meters between two landing-stages. The interference was simulated by a broadband hydroacoustic source placed in a hold of one of the landing-stages. The experiment parameters were as follows: the distance between hydrophones d=0,19 m; the sampling frequency $F_s = 23{,}84$ Hz, the signal frequency $F_c = 1025$ Hz. On the left, the conventional spatial spectra of the signals are presented for the cases when the localized interference source was switched off (dashed line) and on (solid line). On the right, the conventional spectra of the corresponding model signals obtained from the approximation of the Capon spectra of the received signal are shown. The error of the isotropic noise level estimate can be obtained from the difference between the levels of central regions of the model spectra. In the case considered, the error is not greater than 1 dB. This confirms the efficiency of the method presented.

[1] Haykin S. Nonlinear methods of spectral analysis.– Berlin: Springer-Verlag. 1983, 260 p.
[2] Cox H. // J. Acoust. Soc. Am. 1973. V.54. P.1289.

A MATHEMATICAL MODEL OF TWO INTERACTING NEURONS ON ACTIVE TRANSISTOR SUBSTRATE

E.O. Morozova, V.B. Kazantsev

Nizhny Novgorod State University

Investigation of neuroelectronic interfacing is one of the most significant interdisciplinary tasks in modern science with promising implications for the development of new medical diagnostics and treatment devices based on electronic implants.

Nerve cells or neurons are electrically excitable cells. It has been recently shown that such cells can communicate with silicon chip providing the so-called neuroelectronic

interfacing. In our work we consider noninvasive two-way contacts between neurons in vitro and a semiconductor substrate. The cell-silicon junction forms a planar electrical core-coat conductor: the coats of silicon dioxide and membrane insulate the core of the conductive cleft from the conducting environments of silicon and cytoplasm [1]. In such hybrid neuroelectronic system it is possible to implement signal transmission between microelectronics and the microionics of nerve cells in both directions.

The development of neuroelectronic interfacing requires two basic steps. First we need to simulate transistor based recording of individual neuron signals. Next we generate a feedback in the form of capacitive stimulation of an individual cell and follow the response signal propagation between synaptically coupled neurons on the substrate. Then, the model is constructed in the form of two neurons with local capacitive input, signal transmission line (e.g. inter-neuron synaptic coupling) and transistor recording at a second neuron. In such model architecture we can also simulate the interface with microelectronic processing when a nerve pulse from one cell is recorded by the transistor, then the signal travels via a microelectronic circuit in the substrate and finally generates a capacitive input to the second neuron.

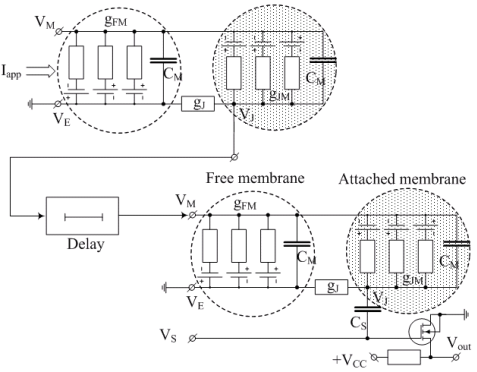

Fig. 1

The zero-dimensional point-contact model is used to describe current and voltage in a core-coat conductor. For illustration we present the model in the form of an equivalent circuit shown in the Fig. 1.

The system of equations is obtained using Kirchhoff's laws. These equations together describe the coupled dynamics of the intracellular and extracellular potentials for the point-contact model. The Hodgkin-Huxley model, taking into account the influence of potential in the electrolyte, is used to describe the dynamics of the membrane potential $V_M(t)$ and the current $I_M(t)$ through a cell membrane in presynaptic and postsynaptic neu-

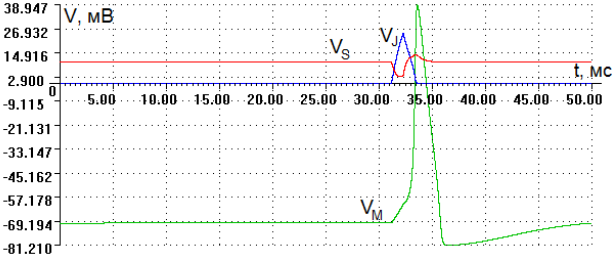

Fig. 2

rons to the electrolyte [2, 3]. Time traces of the membrane potentials of presynaptic and postsynaptic neurons, potential in the electrolyte and transistor gate potential for different conditions were obtained. Figure 2 shows dependences of potential in the electrolyte and transistor gate potential on time. Note that our graphs match the experimental data described in our reference literature [1], which indicates that this model appropriately describes processes in this system.

Future research will include the investigation of large neuronal network interfacing and the construction of a mathematical model, as well as conduction of the experiment using nerve cells from the hippocampus of laboratory rats.

[1] Fromherz P. Nanoelectronics and information technology. / Ed. Rainer Waser. – Berlin: Wiley-WCH. 2003. P.781.
[2] Izhikevich E.M. Dynamical system in neuroscience: the geometry of excitability and bursting. – Mass.: MIT Press, 2007.
[3] Rubin A.B. Biofizika. Biophysics of Cellular Processes. – M.: High School. 1987, 303 p.

THE METHOD FOR IDENTIFYING REPEATING SPATIO-TEMPORAL BIOELECTRIC DISCHARGES IN NEURAL NETWORKS

I.A. Kastalskiy[1,2], A.S. Pimashkin[1,2], S.A. Lobov[2], V.B. Kazantsev[1,2]

[1] *Nizhny Novgorod State University*
[2] *Institute of Applied Physics of RAS*

Modern neuroscience integrates a considerable number of problems requiring a multidisciplinary approach to address them. One of these is the task of identifying activity mechanisms of the brain subsystems. These include the principles of encoding, storing and processing information, which is believed to be encoded in the pulse sequences of spontaneous electrical activity of neural networks.

The studies conducted using the multielectrode array technology for recording biopotentials showed that the slice of neuronal cultures in vitro is also characteristic of the natural intercellular signaling. By using the methods of nonlinear dynamics and statistical radiophysics some regularity in the processes of generation and distribution network discharges were discovered. The presence of repetitive wave-patterns of activation (start of synchronous pulses of all the channels) was statistically revealed. The effect of similarity of reproducible spatio-temporal structures in the neural network could be a key in specifying the relationship between the topological and functional parameters of neural networks and their synaptic contacts, such as connectivity, clustering, etc.

Nowadays a large number of network models for self-oscillator-type neuron-like elements have been developed. One of the main parameters is the membrane cell potential. It has been found that, despite the roughness of such

high-dimensional nonlinear systems, they are also characterized by the dynamic regimes observed in natural biological systems.

There are many methods of bioelectrical activity analysis and classification. A new universal method for processing the multi-channel data has been proposed as a part of radiophysics approach. This method consists in the parallel analysis of waveforms that are converted into a binary raster diagram. We further search for the time limits of a synchronous impulse activity (bursts). To compare the activation patterns of the bursts we have introduced a similar measure for the distance norm in a metric space (the dimension corresponds to the number of registration channels of the cell potential). Using the principles of the cluster analysis we separate and distinguish certain groups containing network discharges close to each other in form.

This new method was verified applying real neural culture data. The applicability of the method to processing obtained data from the model with synaptic plasticity was successfully proved.

This work was supported by the Federal Agency of Science and Innovations (government contracts № 14.740.11.0075, 16.512.11.2136), by the grant of the President of Russian Federation (grant № MD-5096.2011.2), by the RAS Presidium program «Molecular and cellular biology».

[1] Raichman N., Ben-Jacob E. // J. of Neuroscience Methods. 2008. V.170. P. 96.
[2] Мухина И.В., Иудин Д.И., Захаров Ю.Н., Симонов А.Ю., Пимашкин А.С., Казанцев В.Б. // В кн.: Труды научной сессии НИЯУ МИФИ-2010. 2010. Т.3. С.184.
[3] Лебедев Р.Д., Бурцев М.С. // Сб. научных трудов XII Всероссийской научно-технической конференции «Нейроинформатика 2010». В 2-х частях. Ч.1. – М.: НИЯУ МИФИ, 2010. С. 296.

BLOCK DIAGONALIZATION COORDINATED BEAMFORMING SCHEME FOR MULTI-CELL LIMITED FEEDBACK

G. V. Morozov, A. V. Davydov

Nizhny Novgorod State University

In a multi-cell deployment scenario, co-channel inter-cell interference is one of the main factors that limit the performance of wireless cellular systems. The use of effective interference mitigation techniques is essential for avoiding such interference and achieves high system performance gains. The traditional approach to co-channel interference mitigation relies on coordination of physical resources in time and frequency across multiple cells. Recently, spatial domain beamforming schemes with inter-cell coordination have been considered as effective means for co-channel interference mitigation. In this work a novel beamforming scheme for coordinated multi-point downlink transmission is described. The scheme is based on QR matrix decomposition and supports transmission with multiple spatial layers.

A model of the cellular communication system considered here is depicted in the Figure. For the sake of simplicity, there are two coordinating base stations, BS_1 and BS_2, connected to each other via a backhaul link. Base station BS_1 is serving $User_1$ and base station BS_2 is serving $User_2$. Both base stations employ multiple transmitting antennas with adaptive beamforming and coordination. In this deployment BS_1 and BS_2 create significant interference to each other's users due to simultaneous downlink transmission over the same time-frequency resources.

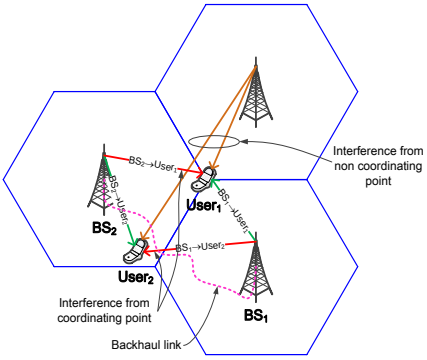

Fig.

Let's consider beamforming at BS_1 to minimize its interference to $User_2$ served by BS_2. The conventional principle of coordinated multi-point transmission is based on Zero Forcing (ZF) beamforming [1]. A matrix of ZF beamforming vectors calculated at the base station is shown in equation (1):

$$\mathbf{W} = \left[\mathbf{W}^{(BS_1 \to U_1)} \mathbf{W}^{(BS_1 \to U_2)}\right] = \mathbf{V}\left(\mathbf{V}^H \mathbf{V}\right)^{-1}. \quad (1)$$

Here, $\mathbf{V} = \left[\mathbf{V}^{(BS_1 \to U_1)} \mathbf{V}^{(BS_1 \to U_2)}\right]$ is a concatenation of principal eigenvectors of $User_1$'s and $User_2$'s channel matrices. In this case, matrix $\mathbf{V}^{(BS_1 \to U_1)}$ is reported directly from $User_1$ to BS_1, whereas matrix $\mathbf{V}^{(BS_1 \to U_2)}$, approximating the interference space of BS_1, is reported from $User_2$ to its serving base station BS_2 and then provided to BS_1 by using the backhaul link between BS_1 and BS_2. Matrix $\mathbf{W}^{(BS_1 \to U_1)}$ is the target beamforming matrix at the serving base station BS_1. Matrix $\mathbf{W}^{(BS_1 \to U_2)}$ isn't used because BS_1 doesn't serve $User_2$.

ZF beamforming doesn't allow any interference between multiple spatial layers including the spatial layers of the same base station when multi-rank transmission is used [1]. However, the complete decoupling of multiple spatial layers at the cost of antenna pattern gain reduction in the direction of the served user is suboptimal when the user is equipped with multiple receiving antennas and can perform its own processing.

In this work we propose a novel beamforming scheme for the coordinated multi-point transmission based on QR decomposition, which is shown in equation (2):

$$\mathbf{V} = \left[\mathbf{V}^{(BS_1 \to U_2)} \mathbf{V}^{(BS_1 \to U_1)}\right] = \mathbf{Q}\mathbf{R}. \quad (2)$$

Here $\mathbf{Q} = \left[\mathbf{Q}^{(BS_1 \to U_2)} \mathbf{Q}^{(BS_1 \to U_1)}\right]$ is a unitary matrix and $\mathbf{R}$ is an upper triangular matrix. Matrix $\mathbf{Q}^{(BS_1 \to U_1)}$ is the target beamforming matrix at the serving base station BS_1. From

equation (3) it can be seen that the QR-based beamforming guarantees the interference suppression from BS_1 to $User_2$:

$$\mathbf{Q}^{(BS_1 \to U_1)^H} \mathbf{V}^{(BS_1 \to U_2)} = \mathbf{0}\,. \qquad (3)$$

At the same time, in comparison with the conventional ZF beamforming, it allows interference among different spatial layers from the same base station.

To evaluate the performance of the proposed QR-based beamforming scheme the system-level simulation of Long-Term Evolution (LTE) Release-10 communication system has been done. The simulation includes Single User Multiple Input Multiple Output (SU-MIMO) mode with up to 2 spatial layers per user under 3GPP Case-1 channel model with the angular spread of 8 degrees [2]. For each user the measurement set for reporting the beamforming matrices consists of the serving cell and a maximum of two interfering cells from the three cells of the same site. The simulation results with average cell spectral efficiency (SE) and cell-edge user SE are shown in the Table.

Table

Scenario	Avg Cell SE, bps/Hz	Cell-Edge User SE, bps/Hz
w/o coordination	2,32 (0%)	0,081 (0%)
conventional ZF	2,57 (+10,8%)	0,085 (+4,9%)
proposed QR	2,67 (+15,0%)	0,087 (+7,4%)

The results presented show that the proposed scheme provides the moderate performance improvement in the cell-edge user SE due to the single layer transmission, where the conventional and the proposed beamforming schemes are identical. A more remarkable gain over the conventional coordinated ZF beamforming is observed for the average cell SE due to the users with the moderate to high data rates which are served in multi-rank transmission mode in most of the cases.

[1] Spencer Q. et al //IEEE Trans. Sig. Process. 2004. V.52. No.2. P. 461.
[2] 3GPP TR 25.996. V.8.0.0. Dec. 2008.

INVESTIGATIONS OF MFM TIP INDUCED REMAGNETIZATION PROCESSES IN FERROMAGNETIC CROSS-SHAPED PARTICLES

M.S. Doronin[1, 2], B.A. Gribkov[2]

[1]*Nizhny Novgorod State University*
[2]*Institute for Physics of Microstructures RAS*

This work is devoted to investigating magnetic force microscopy (MFM) tip induced remagnetization processes of ferromagnetic cross-shaped particles, in particular when investigating the possibility of antivortex state formation in these particles induced by MFM tip. Earlier antivortex magnetization distribution for asymmetric cross-shaped particles was shown to be obtained after the action of an external uniform magnetic field. However, in this case there is a serious problem. This is the complexity of manufacturing

these particles because realization of the antivortex state dramatically depends on the shape of an asymmetric particle [1].

However, there is an easier way to create antivortex state, based on the work with the symmetric cross-shaped particles under the action of an inhomogeneous magnetic field of MFM tip. Accordingly, the requirements for the size and shape of crosses are significantly reduced, which means the technological simplicity of the creation of such particles.

The investigated particles were produced by the electron beam lithography. Lateral sizes of these particles are about 1x1 μm. The main magnetization state of such particles is quasi-homogeneous. The ability of rotating magnetization vector by 90 degrees, induced by the MFM tip, was demonstrated (Fig. 1). The typical height of scanning over the sample surface for remagnetization ability was about 50 nm.

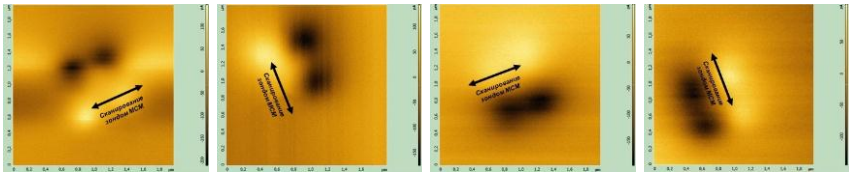

Fig. 1. Rotation of the magnetization vector by 90 degrees. Arrows indicate the direction of moving the MFM tip, allowing to rotate the magnetization vector. View source – from left to right.

The process of MFM tip induced formation of antivortex state in the symmetrical cross- shaped particle was proposed (Fig. 2). It should be noted that the trajectory of the MFM tip goes over two cross segments near the center of the particle.

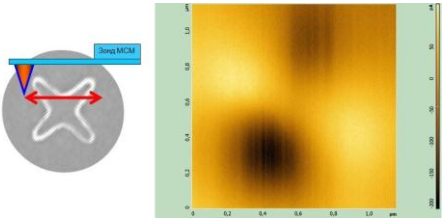

Fig. 2. Trajectory of moving the MFM tip for the formation of the antivortex magnetization state (left). The result of the remagnetization process (right).

Micromagnetic computer simulation (based on program SIMMAG, IPM RAS) of the antivortex formation process in the symmetric cross-shaped particle under the action MFM tip field was carried out (Fig. 3). Initially the particle was in the quasi-homogeneous state (Fig. 3, left). Further the tip is moving over the particle. The tip is seen to start disturbing the magnetization distribution and it is shifting (“pulling”) it to itself. The direction of the magnetization vector of the left cross segment is reversed (Fig. 3, middle). After the tip comes out of the zone of the particle, the magnetization distribution begins to relax, resulting in the antivortex magnetization distribution in the symmetrical cross-shaped particle (Fig. 3, right).

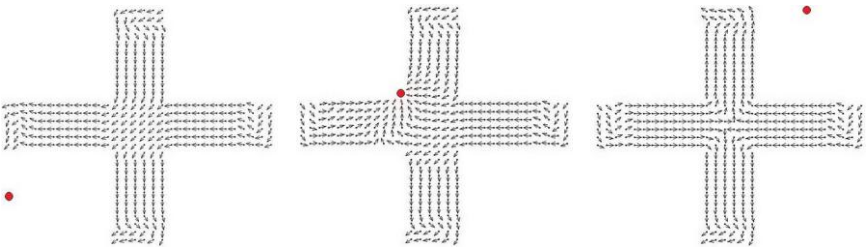

Fig. 3. A quasi-homogeneous magnetization state (left), an intermediate state (middle), an antivortex magnetization state (right).

Thus, the possibility of the MFM tip induced rotation of the magnetization vector of the symmetric quasiuniform cross-shaped Co particles was shown. We propose a method for forming the antivortex distribution of magnetization in the crosses under the action of the MFM tip.

[1] Mironov V.L., Ermolaeva O.L., Gusev S.A., Klimov A.Yu., Rogov V.V., Gribkov B.A., Udalov O.G. and Fraerman A.A. // Phys. Rev. B. 2010. V.81. P. 094436.